EBG enhanced feeds for the improvement of the aperture efficiency of reflector antennas

EBG Enhanced Feeds for the Improvement of the Aperture Efficiency of Reflector Antennas

Andrea Neto, *Member, IEEE*, Nuria Llombart, *Member, IEEE*, Giampiero Gerini, *Member, IEEE*, Magnus D. Bonnedal, *Member, IEEE*, and Peter de Maagt, *Senior Member, IEEE*

***Abstract*—We describe the use of electromagnetic bandgap (EBG) super-layers to improve the shape of reflectors illumination function. Following an investigation of the leaky wave pole singularities of the EBG Green's function, the shape of the radiation patterns of small apertures in ground planes are optimized. The maximization of the reflector aperture efficiency can be obtained by properly tuning the super layers geometrical parameters. A prototype of such feed has been designed, manufactured and tested. The results indicate that the inclusion of the EBG, increases the aperture efficiency of the feed+reflector system to values higher than 80%, over a 10% bandwidth. These low profile feeds are compatible with printed circuit board and/or integrated technology.**

***Index Terms*—Aperture efficiency, electromagnetic bandgap (EBG) materials, leaky waves, reflector antenna feeds.**

I. Introduction

REFLECTOR antenna systems have been thoroughly investigated for decades and represent a mature technology [1]. Major improvements in their performance cannot be realistically expected. Typically the feeds of the reflectors are realized with high performance corrugated horns [2] that can be optimized for high efficiency, high gain, low cross polarization, high or low focal to diameter (F/D) ratio, etc.

Especially at low frequencies, typical feed horns can be lengthy and bulky. At the opposite end of the spectrum, at millimeter or sub-millimeter wave frequencies, the horns can be difficult to manufacture. These aspects constitute a significant drive to find alternative technologies, that can be used to obtain equally performing feeds. In particular it is useful to explore the possibility of using integrated technology to upgrade the performances of a moderately sized (in terms of the wavelength) waveguide horn, so that the resulting feed can be used to efficiently illuminate a reflector antenna.

Recent investigations seem to indicate that electromagnetic bandgap (EBG) super-layers could be used to obtain this goal. In [3]–[5], it was indicated that EBG super-strates could be adopted to increase the directivity of an aperture that is small in terms of the wavelength. In [6], the bandwidth (BW)-gain tradeoff for these same structures was discussed. However the directivity alone is not sufficient to qualify a feed pattern as good to feed a reflector antenna, especially for medium or small F/D ratios. The two dominant feed-dependent factors that contribute to the aperture efficiency [7] are spill over ($\eta_{\rm sp}$) and taper efficiency ($\eta_{\rm tap}$). It is well known that reducing the spill over with a highly directive feed, that creates a low edge taper, will result in a poor taper efficiency. Accordingly a compromise between the two must emerge. In this paper, the use of EBG dielectric super-layers is proposed to improve the small aperture pattern by shaping it rather than by increasing the directivity only.

In this scope, the Green's function of the EBG superstructure is investigated in detail. From its spectral representation, the most significant leaky pole contributions are extracted and their role in defining the shape of the far field pattern of an underlying feed is described. Inverting this procedure, starting from a required radiation pattern, one can identify the pertinent geometrical parameters that lead to the desired leaky wave poles. An angular filtering effect that maximizes the reflector efficiency can be obtained. In this paper the canonical case of a center fed reflector is considered. However the shaping of the pattern via leaky waves is of general applicability and no specific application is targeted. An unrealistic but theoretically optimum pattern would be characterized by $sec^4(\theta/2)$, [7]. Such pattern will be pursued to the best that the proposed EBG technology allows.

The term aperture efficiency will be used to indicate the product of the spill over efficiency $\eta_{\rm sp}$, the taper efficiency $\eta_{\rm tap}$, the phase efficiency η_{ph} and the polarization efficiency $\eta_{\rm pol}$: $\eta_{\rm ap} = \eta_{\rm sp}\eta_{\rm tap}\eta_{ph}\eta_{\rm pol}$. For the definitions in this paper we refer to [7]. These parameters are mostly associated to the relation between the feed pattern and the *F*ocal distance to *D*iameter (F/D) ratio of the reflector.

Since center-fed reflectors will be considered, another factor to be accounted for is the blockage efficiency $\eta_{\rm bl}$. The latter largely depends on the actual ratio of the areas of the reflectors and the feed weighted by the feed pattern. When the blockage is included the efficiency figures refer to $\eta_{\rm tot} = \eta_{\rm ap}\eta_{\rm bl}$. The feed supports could also have an effect in center-fed reflectors, however they are not accounted for in this paper.

II. Polar Representation of the Radiated Field

The geometry of the feed under investigation is described in Fig. 1. It consists of a square metallic waveguide opening in a infinitely extended ground plane covered by a period arrangement of infinite dielectric layers. Note that the effects of the finiteness of the ground plane and of the dielectric slabs will be accounted

Manuscript received September 4, 2006; revised April 24, 2007. This work was performed under contract with the European Space Agency: Photonic Bandgap Terminal Antennas (Contract A0/1-4636/04/NL/GA).

A. Neto, N. Llombart, and G. Gerini are with TNO Defence, Security and Safety, Den Haag 2597 AK, The Netherlands (e-mail: andrea.neto; nuria.llombartjuan; giampiero.gerini@tno.nl).

M. Bonnedal is with Saab Ericsson Space AB SE-405, 15 Goteborg, Sweden (e-mail: magnus.bonnedal@space.se).

P. de Maagt is with the Electromagnetics Division, European Space Agency, 2200 AG, Noordwijk, The Netherlands (e-mail: Peter.de.Maagt@esa.int).

Digital Object Identifier 10.1109/TAP.2007.901854

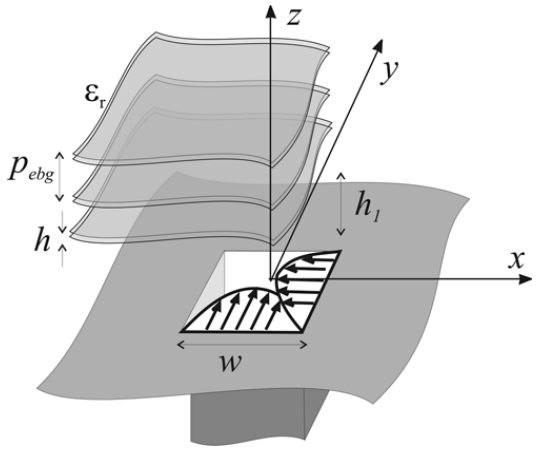

Fig. 1. Square metallic waveguide of dimension w in a infinitely extended ground plane covered by a period arrangement of infinite dielectric layers. The dielectric layers have a thickness h and dielectric constant ϵ_r, while period between them is p_{ebg}. The distance between the ground plane and the first dielectric layer is h_1.

for in the final analysis stage rather than in the following preliminary design phase. The reference system has its z axis normal to the ground plane and to the dielectric stratifications, the geometrical parameters are specified in the inset and the magnetic currents, $m(x,y)$, are representative of the electric field distribution associated with the waveguide. For simplicity, in this paper we will consider only the two orthogonal TE_{10} modes. This approximation will appear to be valid taking into account the long tapering of the feeding waveguide eventually implemented.

A. Spectral Green's Function

The electric or magnetic fields radiated by an elementary magnetic current in the presence of the multilayered dielectric structure and of the ground plane are most compactly expressed as inverse Fourier transforms of the spectral Green's functions. In this section we will consider the electric field radiated at $\mathbf{r}(\rho,\phi,z)=\mathbf{r}(r,\theta,\phi)$ in the region of space above the EBG dielectric stratifications. Accordingly the o component of the observed electric field radiated by the s component of the source magnetic current can be expressed as follows:

$$e_o(\mathbf{r}) = \frac{1}{(2\pi)^2}\int_0^{\infty}\int_0^{2\pi} G_{o,s}^{\mathrm{em}} M_s e^{-jk_\rho\rho\cos(\alpha-\phi)} e^{-jk_{z0}z} k_\rho d\alpha dk_\rho \tag{1}$$

where k_ρ and α are the spectral variables. $G_{o,s}^{\mathrm{em}} = G_{o,s}^{\mathrm{em}}(V_{\mathrm{TE}}, V_{\mathrm{TM}}, k_\rho, \alpha)$ is the spectral Green's function (GF). $V_{\mathrm{TE}}, V_{\mathrm{TM}}$ are the TE and TM potential functions, that are obtained as voltage solutions of the pertinent transmission lines with series unitary voltage generators. Note that the two potentials are functions of k_ρ only. $M_s(k_\rho,\alpha)$ is the Fourier Transform (FT) of $m(x,y)$ and $k_{z0}=\sqrt{k_0^2-k_\rho^2}$. The analytic expressions of these spectral functions can be found in the appendix for the sake of completeness.

It is well known that when the observation point is at large distance from the dielectric stratifications, a simple uniform asymptotic evaluation of the field can be performed, see [8, Appendix B-1], and this leads to

$$e_o(\mathbf{r}) = G_{o,s}^{\mathrm{em}}(V_{\mathrm{TE}}, V_{\mathrm{TM}}, k_0\sin\theta, \phi) \cdot M_s(k_0\sin\theta,\phi) 2jk_0\cos\theta \frac{e^{-jk_0 r}}{4\pi r}. \tag{2}$$

The shape of the field is directly proportional to the product of the two spectral functions $G_{o,s}^{\mathrm{em}}$ and M_s evaluated for the real values of $k_\rho = k_0\sin\theta$, and $\alpha=\phi$. This evaluation, based only on the branch point contribution, is valid due to the fact that the potential functions of planar stratified structures are analytic in the surrounding of the origin ($|k_\rho| < k_0$) except for a few isolated polar singularities, that cannot become infinite when evaluated for real values of k_ρ. These singularities represent the leaky wave poles.

B. Polar Approximation of the GF

The analysis of the leaky wave pole solutions associated to the GF of dielectric stratified geometries has been the object of several in depth studies such as [9] and there cited references. More specifically, the detailed study in [10] introduced the general concept that the broadside directivity of antennas can be enhanced by placing a series of quarter dielectric wavelength slabs at a distance of a quarter free space wavelength from each other. This concept was then used by others, [3]–[5] to obtain EBG based highly directive antennas. The propagation constant of each leaky wave pole is defined by the zeros of the denominators of the potential functions V_{TE}, V_{TM}. It is useful to express a leaky wave pole as $k_{lw}=k_0(\sin\theta_{lw}+j\delta_{lw})$. Even if the structures studied in the cited references were composed by multiple dielectric layers, in all cases only one leaky wave pole was actually used to enhance the broadside radiation ($\theta_{lw}\approx 0$). In the present work, the aim is to provide guidelines on how to achieve a predefined pattern which may require more than one pole to be excited and most likely these poles will need to point at directions $\theta_{lw}\neq 0$.

Since the voltages can be expressed as $V_{\mathrm{TE/TM}}(k_\rho) = N(k_\rho)/D(k_\rho)$, the residues at the poles locations, $\mathrm{Res}(V_{\mathrm{TE/TM}})(k_{lw})$ can be calculated as $N(k_{lw})/D'(k_{lw})$ where the prime denotes derivation with respect to k_ρ. The explicit form of this derivative will depend on the specific stratification. However in all cases the denominator $D(k_\rho)$ includes the functions k_{z0} and $k_{z1}=\sqrt{\epsilon_r k_0^2-k_\rho^2}$. Thus the derivatives $D'(k_{lw})$ are explicitly proportional to $k_{lw}=k_0(\sin\theta_{lw}+j\delta_{lw})$. As a consequence the magnitudes of the residues are higher for smaller pointing angles when δ_{lw}, the attenuation constant, is very small. The potentials can be directly approximated in the surrounding of the pth pole, namely k_{lwp}, using the residue theory as follows:

$$V_{\mathrm{TE/TM}}(k_\rho)_{|k_\rho\approx k_{lwp}} \approx V_{\mathrm{TE/TM}}^{lwp}(k_\rho) = \frac{2k_{lwp}}{k_\rho^2-k_{lwp}^2}\mathrm{Res}(V_{\mathrm{TE/TM}})(k_{lwp}). \tag{3}$$

The functions $F_{\mathrm{TE/TM}}(k_\rho) = V_{\mathrm{TE/TM}}(k_\rho) - \sum_{p=1}^{N_p}(V^{lwp}_{\mathrm{TE/TM}}(k_\rho))$ are analytic in the entire domain ($|k_\rho| < k_0$). This implies that $F_{\mathrm{TE/TM}}$ can be well approximated by a power series expansions around ($k_\rho = 0$). Retaining only the first term of such series, $F_{\mathrm{TE/TM}}(0)$, a convenient expansion for the original potentials is found to be

$$V_{\mathrm{TE/TM}}(k_\rho) \approx F_{\mathrm{TE/TM}}(0) + \sum_{p=1}^{N_p}(V^{lwp}_{\mathrm{TE/TM}}(k_\rho)). \quad (4)$$

The convenience of this representation, even considering that the starting point were analytically known potentials, is that the contribution of each term to the far field pattern can be isolated as associated to a specific design parameter. In fact a pole is dominant in a certain angular domain of the pattern, around θ_{lw} when it has a small imaginary part. When N_p poles are dominant, the radiation pattern can be synthesized as superposition of the pertinent residues using (2) where the potentials are approximated as in (4). The present approximation extends the validity of the one found in [11] [(2) and (3)], to include also the cases where the excitation of the leaky waves is less dominant. In these cases the contribution associated to space waves radiated directly from the source is also significant and accounted for by the term $F_{\mathrm{TE/TM}}(0)$.

C. EBG Design

As explained in [12] the highest directivity at broadside, associated to potential functions presenting a single leaky wave pole for $k_{lw} \approx 0$, is obtained when the distance between subsequent dielectric slabs, p_{ebg} is in the order of $\lambda_0/4$ and $h_1 \approx \lambda_0/2$. When the parameter h_1 is increased to $h_1 > \lambda_0/2$ a leaky wave pole is still found for each polarization (TE or TM) but its real part is such that the main direction of radiation is shifted away from broadside.

The number of leaky wave poles changes when the parameter p_{ebg} grows to $p_{\mathrm{ebg}} = \lambda_0/2$. A second leaky wave pole (for each polarization) becomes relevant (i.e., its imaginary part becomes small). In Fig. 2 the propagation constants of the leaky wave pole solutions of the dispersion equation of an EBG structure composed of two layers with $\epsilon_r = 2.2$ are shown. Fig. 2(a) shows the radiation angles associated to these poles, while Fig. 2(b) shows the corresponding attenuation constants. For TE polarization two leaky wave poles are found pointing to different θ directions, ($\theta \approx 10°$) and ($\theta \approx 34°$) at the central frequency. Two poles pointing in similar directions are found also for TM polarization. Note that the dominant among these two poles in each polarization is the $\mathrm{TE}_2/\mathrm{TM}_2$ because its attenuation constant is significantly closer to zero. However, the TM case polarization introduces also a third pole that peaks at larger observation angles (around 60° in the example).

The convenience of the two poles configuration is that it consents to shape the radiation patterns from these EBG super-layered kind of structures. Both E and H planes patterns associated to the structure of Fig. 2, excited by a square waveguide with dimension $l = 0.7\lambda_0$ at the center of the investigated bandwidth, are shown in Fig. 3. The graphs compare the results achieved retaining the complete GF asymptotic evaluation, (2), and its

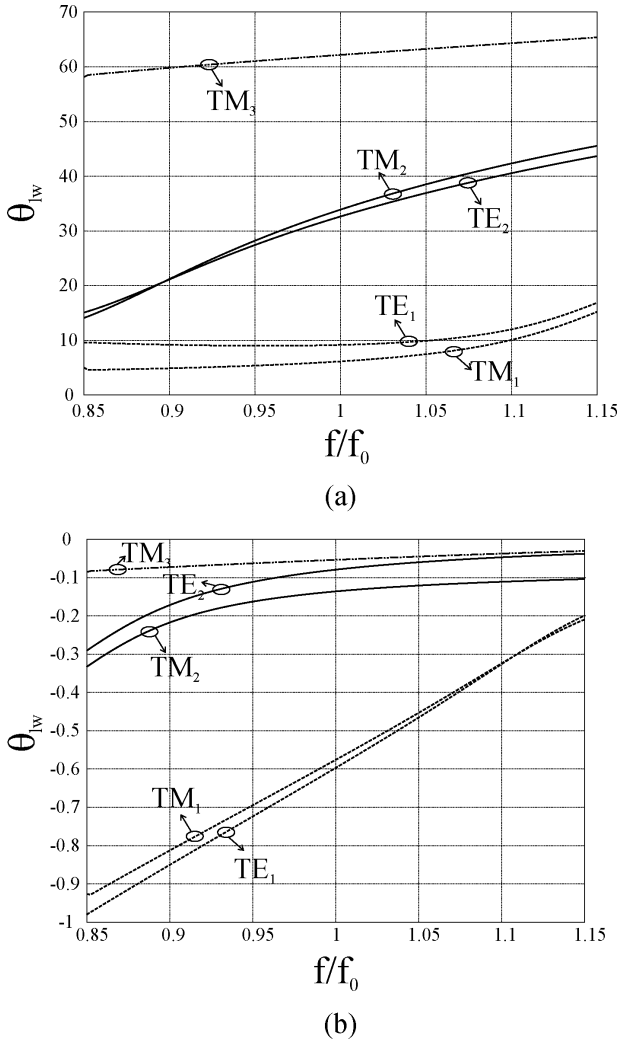

Fig. 2. Solutions of the dispersion equation for an EBG composed of two layers with $\epsilon_r = 2.2$, $h_1 = 14.1$ mm, $p_{\mathrm{ebg}} = 14.1$ mm, $h = 4.75$ mm, $f_0 = 10.64$ GHz (a) shows the radiation angles θ_{lwn} (b) shows the attenuation constants δ_{lwn}.

approximation. It is apparent that the approximation in (4) is accurate even for a relatively large observation angle θ.

The broadside region is dominated by the space wave and by the poles $\mathrm{TE}_1/\mathrm{TM}_1$ while the angle of strongest radiation is defined by the $\mathrm{TE}_2/\mathrm{TM}_2$ poles (dominant ones). The TM_3 mode that contributes in the E-plane for large observation angles is non desired in the designs that will follow. Precautions will have to be taken in order not to excite it. Even though this pole is present in all dielectric super-layer configurations it is typically neglected by other authors.

III. Input Admittance

The input admittance of the waveguide in Fig. 1 can be rigorously expressed in the spectral domain. Resorting to a cartesian spectral representation similar to that of (1), and understanding that in this context G stands for $G^{hm}_{x,x}$, the input admittance is

$$Y^{\mathrm{ebg}} = \frac{1}{(2\pi)^2}\int_{-\infty}^{\infty}\int_{-\infty}^{\infty}|M(k_x,k_y)|^2 G^{\mathrm{ebg}}(k_x,k_y,z=0)dk_x dk_y. \quad (5)$$

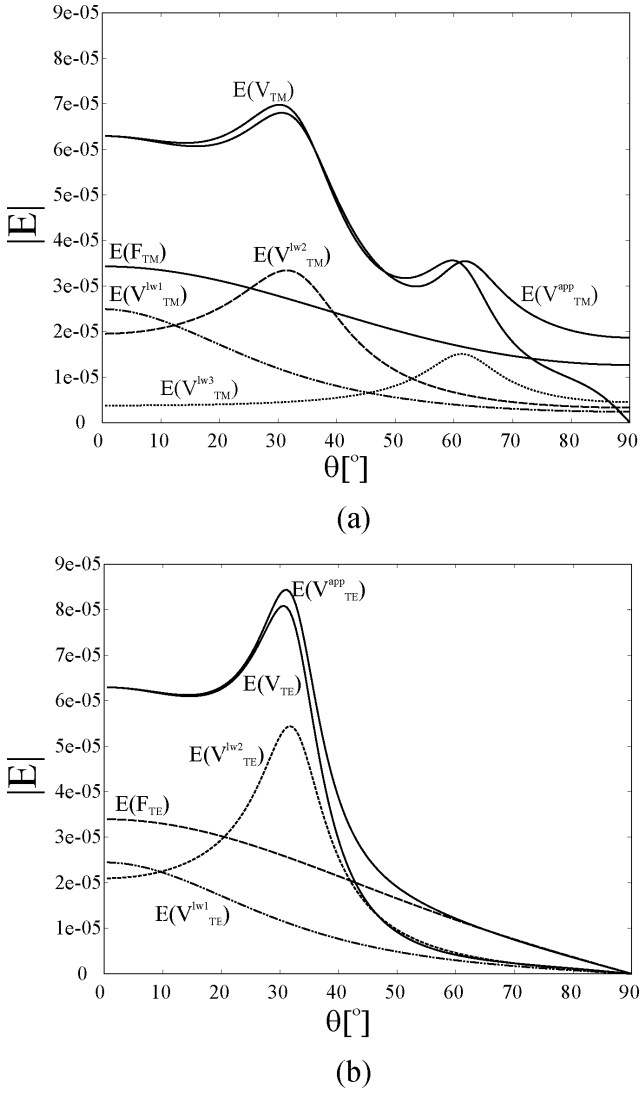

Fig. 3. E and H radiation patterns from the same structure of Fig. 2, excited by a square waveguide with dimension $l = 0.7\lambda_0$ (a) E-plane, (b) H-plane.

Substituting G^{ebg} with the Green's function of free space G^{fs} (grounded), one could obtain the standard aperture admittance, Y^{fs}.

In order to quantify the impact of the EBG super-layers with respect to the free space case and to provide physical insight to the wave mechanism, Fig. 4 presents Y^{ebg} and Y^{fs} as a function of the frequency. The curves were calculated using the full wave analysis tool described in [13]. The difference between the free space and the EBG curves is an oscillation with more than one periodicity, each one defined by the distance between the aperture and the dielectric interfaces.

The amplitude of the oscillations is proportional to the amplitude of the intensity of the excitation of the leaky waves. This amplitude is quantified by the value of the pertinent residue at the dominant pole: $\mathrm{Res}(I_{\mathrm{TE/TM}})(k_{lwp}) \propto 1/\sin\theta_{lwp}$. Correspondingly, the input admittance is varying function of the frequency, with stronger oscillations for broadside pointing configurations. This property is common to all designs that use Fabry–Perot like structures. The enhancement of broadside directivity is achieved at the expense of working bandwidth. The

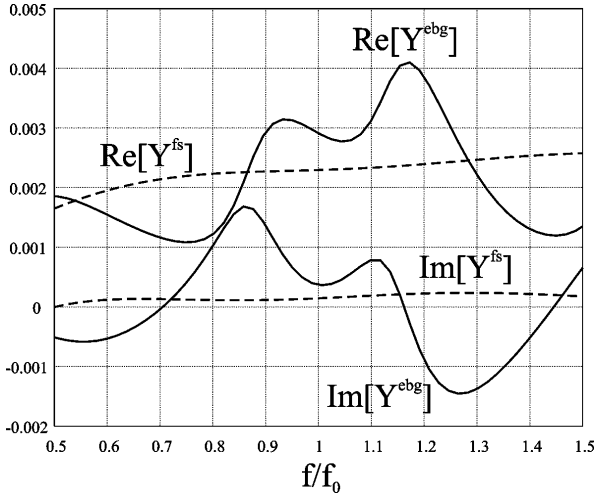

Fig. 4. Admittance of a square waveguide with dimension $l = 1.08\lambda_0$ in the presence of the EBG super-structure of Fig. 3 and in free space.

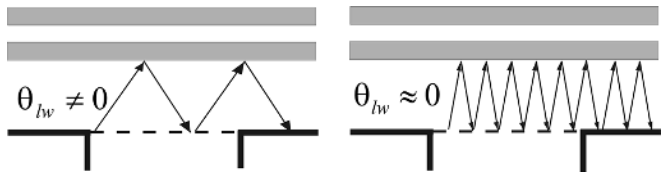

Fig. 5. Ray picture associated to two configurations corresponding to a leaky wave radiating toward a direction clearly different or close to broadside ($\theta_{lw} \approx 0$).

bandwidth behavior can be intuitively understood by observing that when the leaky wave radiates toward broadside more reflections from the dielectric slabs will be directly coupled into the waveguides, than when the leaky wave is pointing toward larger angles, see Fig. 5.

This work exploits the possibility to shape the feed radiation pattern using leaky waves associated with large pointing angles. In fact in the present configuration the input impedance remains comparable over bandwidths in the order of 10%. This is due to the fact that the dominant poles point toward large angles over the entire band (see Fig. 2).

IV. Feed Design for High Efficiency Reflector

In Section II-C we have presented a design that could constitute the preliminary dimensioning of an EBG superstructure to be used to enhance the properties of a center-fed reflector. In fact the patterns in Fig. 3 present a slowly growing amplitude until 35° and a steep roll offs after that angle. To get a first estimation of the quality of this feed its radiation patterns have been used to feed a circularly symmetric reflector. The efficiencies of the ensemble feed + reflector have been calculated using an in house developed code based on standard PO approximation for the reflector radiation integral. The integration is performed over the angular variable associated to the angle subtended by the feed and the relative point on the reflector, θ, which varies from 0 to the angle subtended by the reflector, θ_{sub}. As it is, this feed could be used for a reflector of $\mathrm{F/D} = 0.68$ achieving a good overall aperture efficiency $\eta_{\mathrm{ap}} \approx 73.6\%$.

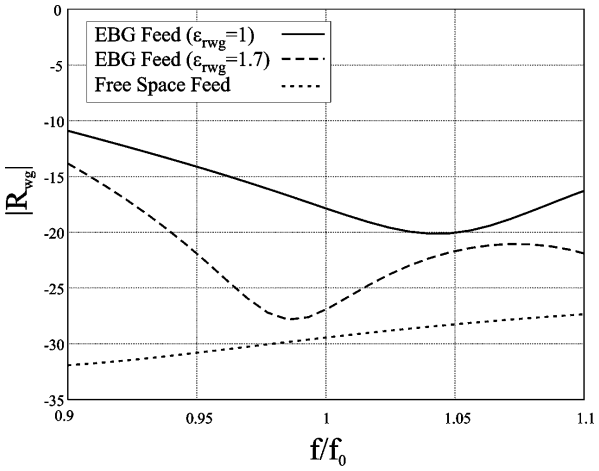

Fig. 6. Reflection coefficient of the final design as a function of the normalized frequency ($\epsilon_r = 2.2$, $h_1 = 14.5$ mm, $p_{\rm ebg} = 13.8$ mm, $h = 4.75$ mm, $f_{0-10.64\ \rm GHz}$). The reflection coefficient of the waveguide in free space is also shown. For a better matching the waveguide can be filled by a low dielectric constant material ($\epsilon_{\rm rwg} = 1.7$).

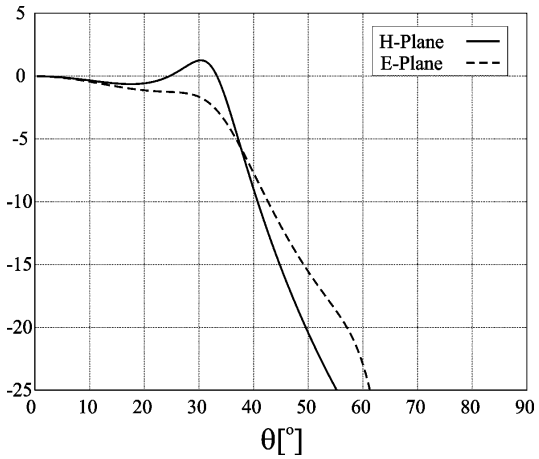

Fig. 7. E and H-plane radiation patterns of the optimized structure of Fig. 6 and at the central frequency.

However, a closer look at this configuration reveals a drawback. The H-plane is well behaved and if it would be possible to maintain the pattern over all ϕ angles the overall aperture efficiency would be 90%. However the E-plane presents a peak of radiation associated to a third pole ($\rm TM_3$) which translates into spill over and therefore reduces the aperture efficiency. This third pole can be cancelled by matching it with a zero of M_s. This can be obtained by enlarging the dimension of the waveguide aperture to about $l = 1.08\lambda_0$. This fine tuning implies a different optimum $\rm F/D = 0.72$.

A. Final Design

As a result of the considerations on the impedance of Section III it is possible to also fine tune the distance between the ground plane and the dielectric layers h_1 so that the external admittance, $Y^{\rm ebg}$, would be real. The calculated reflection coefficient for the new enlarged EBG covered feed is shown in Fig. 6 as a function of the normalized frequency. The case of the waveguide in free space is shown for reference purposes.

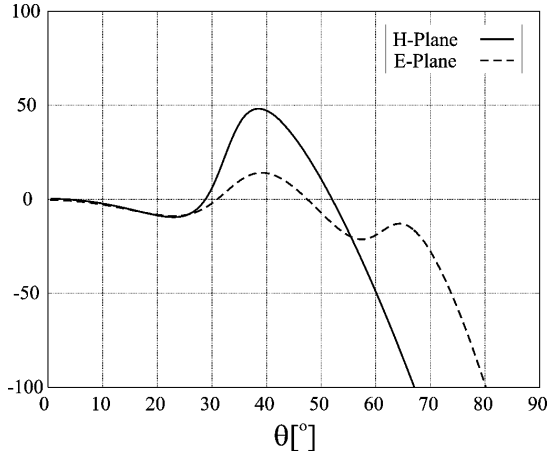

Fig. 8. E and H-plane phase distribution at the reflector aperture of the optimized structure of Fig. 6 and at the central frequency.

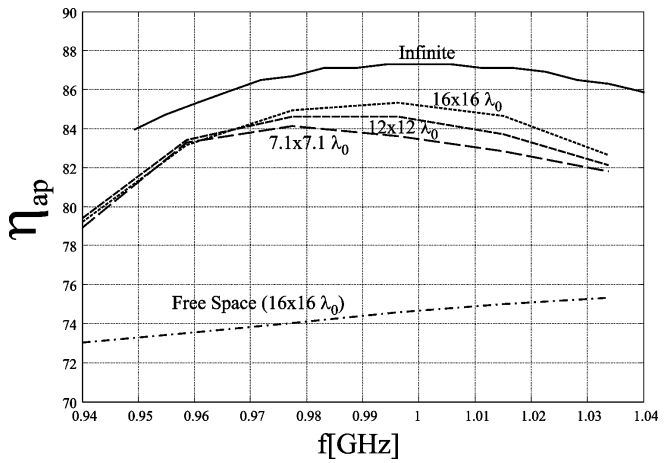

Fig. 9. Aperture efficiency as a function of the normalized frequency, for the different dimensions of the square super-layers. The dimension indicated close to the free space case refers to the dimension of the finite ground plane.

For a better matching of the EBG feed, the $\rm TE_{10}$ waveguide characteristic admittance can be matched to the real part of the external admittance $Y^{\rm ebg}$ by filling the waveguide with a low dielectric constant material ($\epsilon_{\rm rwg} = 1.7$), see Fig. 6.

The optimization of the matching has been performed simultaneously with the optimization of the radiation patterns: that is reducing the distance $p_{\rm ebg}$ to compensate for the shift of the dominant $\rm TE_2/TM_2$ location caused by the increase of h_1. The patterns are shown in Fig. 7 at the central frequency. Since the third pole in the E plane has been suppressed overall lower spill over can be expected. The phase distribution at the reflector aperture is shown in Fig. 8. It is instructive to observe that the maximum variation of the phase is centered around the pointing angle of the dominant leaky wave (in the present example this is around 32° degrees). This phase variation property is a cause of reduction of the aperture efficiency. However, for the present design based on low dielectric constants, the phase variation until 38°, which corresponds to the subtended angle of a reflector with $F/D = 0.72$, is below 50°, thus it is not a major problem. Overall the radiation pattern is well behaved in amplitude and in phase.

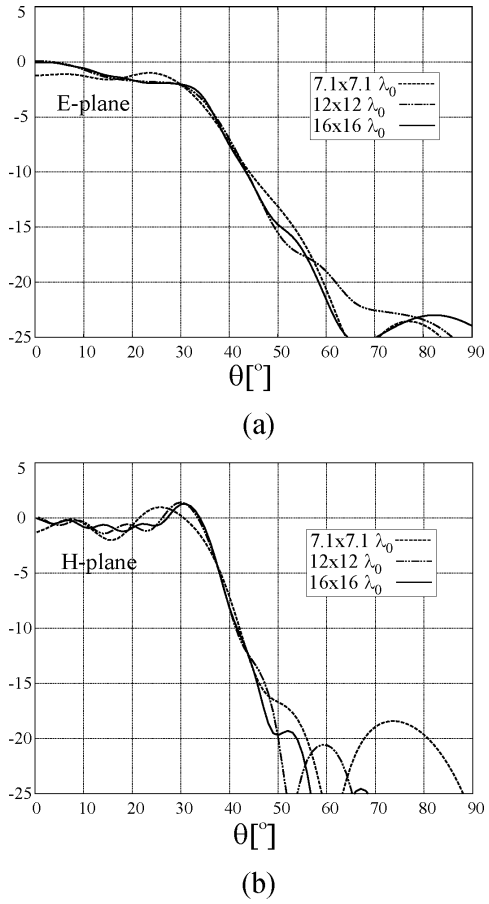

Fig. 10. (a) E and (b) H-plane amplitude distribution at the reflector aperture at the central frequency for several dimensions of the dielectric slabs.

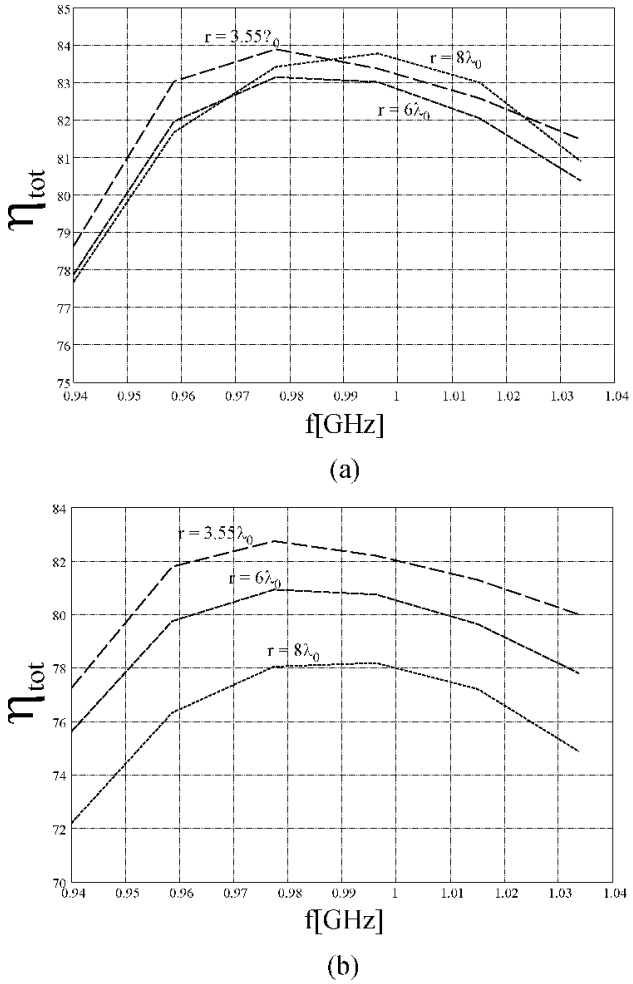

Fig. 11. Total efficiency as a function of the normalized frequency for a reflector diameter of (a) $D = 159\lambda_0$ and (b) $D = 88\lambda_0$.

This feed reflector ensemble reaches an aperture efficiency of $\eta_{\rm ap} = 87.5\%$. As shown in Fig. 9, with the curve marked *infinite*, the high efficiency is obtained over a relatively large BW since $\eta_{\rm ap} > 84\%$ is maintained over a 10% BW.

B. Finiteness Effects

The present design procedure has been entirely based on the use of the EBG GF whose spectrum is known analytically for infinitely extended planar stratifications. However a realistic structure will necessarily be realized with finite dimensions. The attenuation constant of the leaky wave poles is directly linked to the amount of power that travels parallel to the dielectric slabs and eventually reaches their edges. In the present design the dielectric stratifications were realized with low dielectric constant materials which provides relatively large attenuation constants of the leaky waves. Therefore the impact of the diffraction from the edges of the slabs is relatively low. In order to quantify this impact a parametric study has been performed using the commercial code CST MSW [14]. Different slabs dimensions have been considered and the pertinent patterns are shown in Fig. 10. The aperture efficiencies for these same cases are also reported in Fig. 9. The efficiencies of the finite structures are all lower (by at least 2%) than the ones of the infinite structure mainly because the back radiation is now considered. Note that the expected peak efficiencies are 10% higher than they would be in absence of the EBG super-structure. Finally with high quality dielectric materials ($tg\delta < 0.001$) the losses associated to the dielectric appeared to be negligible in the simulations.

C. Impact of Blockage

The previous considerations on the finiteness would not be complete without accounting for the impact of the blockage on the total aperture efficiency. The final selection of the dielectric dimension should be driven by the tradeoff between cleaner pattern shapes and a smaller blockage. This latter is dependent on the ratio between the areas of the main reflector and of the feed weighted by the illumination law. To account for the blockage effect the radiation integral is simply extended from $\theta_{\rm bl}$ to $\theta_{\rm sub}$. Assuming always reflectors characterized by the same F/D ratio, the actual blockage angle for a given feed dimension depends on the diameter D. In Fig. 11(a) and (b) the actual total efficiencies calculated as $\eta_{\rm tot} = \eta_{\rm ap}\eta_{\rm bl}$ are reported for two different reflector diameters: $D = 159\lambda_0$ and $D = 88\lambda_0$. In Fig. 11(a) all feed dimensions (assumed to be circular with radius r) provide high efficiencies. In Fig. 11(b) the highest efficiency is given by the smallest feed radius ($r = 3.55\lambda_0$) since for small reflectors the blockage impact is important.

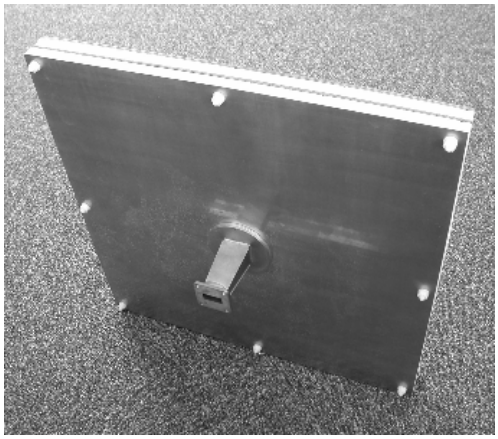

Fig. 12. Photo of the prototype.

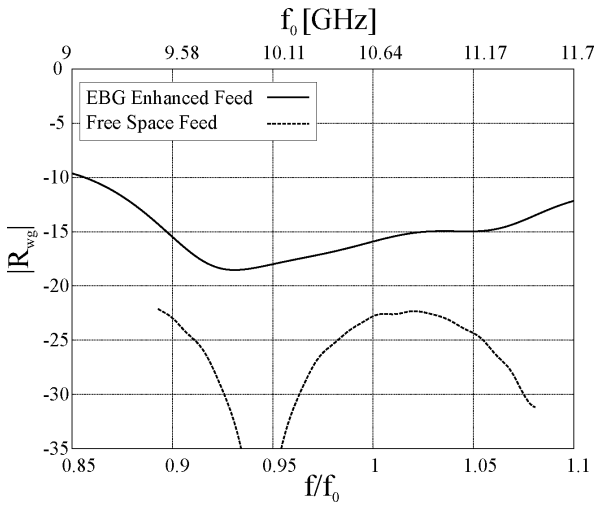

Fig. 13. Measured reflection coefficient at the standard waveguide for the prototype as a function both of the frequency and of the normalized frequency.

V. Prototype Demonstrator

In order to validate the design methodology shown in Section IV a prototype of the EBG enhanced feed has been manufactured, Fig. 12. A standard WR90, *X* band, waveguide (22.86 mm×10.16 mm) is connected to the radiating aperture (30.7 mm×30.7 mm) via a section that was linearly flared in both directions. The largest slab case (450 mm×450 mm equivalent to $16\lambda_0 \times 16\lambda_0$) was chosen for the prototype, since the aim in this paper was to shape the pattern. If one was willing to use this structure for a small reflector diameter, the smallest feed dimension should be used (see Fig. 11). The frequency of operation is centered around 10.64 GHz and spans over a 10% BW. Commercially available dielectric slabs with $\epsilon_r = 2.2$, were separated one from the other and from the ground plane by means of two further foam slabs. The foam was initially thought of as having dielectric constant equal to the one of free space. The reflection coefficient as a function of the frequency has been measured and is shown in Fig. 13. Both the real and the normalized frequency scales are shown in the abscissa (below and above the graph). The two scales highlight that the bandwidth where the realized antenna presents lower reflection coefficient is shifted toward lower frequencies by about 10% (the -15 dB level is achieved in the 9 – 10 GHz band rather than the 10 – 11 GHz band). This significant shift seems to be mainly associated with the following manufacturing imperfections.

- The foam dielectric constant has been measured to be 1.07 rather than 1. This causes a 7% frequency shift in the location of the leaky wave pole;
- The distance between the ground plane and the first EBG layer has been found to be 15 mm rather than the design value of 14.5 mm.

The patterns from the prototype have been measured over a large frequency band showing that the frequency shift is not only in the reflection coefficient but also in the radiated fields. Fig. 14 shows the measured radiation patterns at the edges of the BW (9.4 and 10.2 GHz). Despite the shift in frequency, the patterns are very clean and resemble the designed ones. One can observe the sharp drop off after 35° as expected. The cross polarization levels, according to the third Ludwig definition, are also reported and found to be relatively low.

From the measured feed E and H patterns the efficiencies have been obtained for a center-fed reflector of $\mathrm{F/D} = 0.72$ and are shown in Fig. 15. It is apparent that the bandwidth with aperture efficiency larger than 80% is shifted toward lower frequencies just like the reflection coefficient matching bandwidth. Despite the frequency shift the peak measured efficiency is only 2% lower than the peak predicted efficiency. Fig. 15 also shows the efficiencies associated to calculated feed patterns predicted from numerical simulations that include a value of $\epsilon_r = 1.07$ for the dielectric constant of the foam. These simulations show reasonable resemblance with the measurements indicating, at least partially, the repeatability of the hardware. The matching loss is not included since the matching could be improved by filling the waveguide with a dielectric of $\epsilon_{\mathrm{rwg}} = 1.7$ as shown in Fig. 6. For completeness the blockage impact could be taken into account. The total efficiency for a reflector with $D = 159\lambda_0$ would be 2% lower than the aperture efficiency shown in Fig. 15.

VI. Conclusions

The radiation patterns from standard feeds, e.g., horns, often are as $\cos^n(\theta)$, where n depends on the feed type and aperture size. The aperture efficiency of reflector antennas centrally fed by these patterns standard are, in practice in the 65%–80% range. In this contribution, the aperture efficiencies of the standard feed+reflector systems are enhanced by accurately shaping the patterns to the ideal $sec^4(\theta/2)$, using EBG super layers. Ideally the design presented here could show 87% peak aperture efficiency. It should also be noted is that if the feed is used in a cylindrical reflector system rather than a rotationally symmetric one, 90% efficiency could have been theoretically predicted. In order to provide hardware demonstration of the concept, a prototype EBG based feed has been manufactured and measured. The measured patterns, used as input for an analysis tool that simulates a center fed reflector system, lead to an aperture efficiency larger than 80% over a 10% relative BW. A frequency shift is observed in the measurements, with respect to the design. Its origin has been traced back to manufacturing inaccuracies.

This paper presented results of general applicability without targeting a specific application. However some considerations

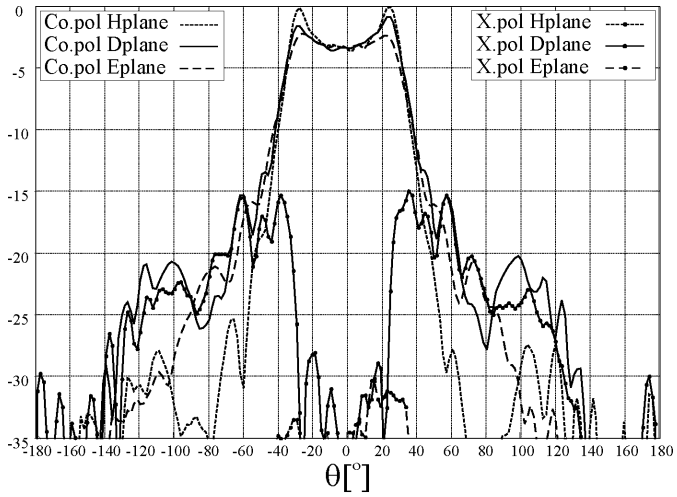

Fig. 14. Measured radiation patterns in the E-, H-, and D-planes at the edges of the BW: (a) 9.4 GHz and (b) 10.2 GHz.

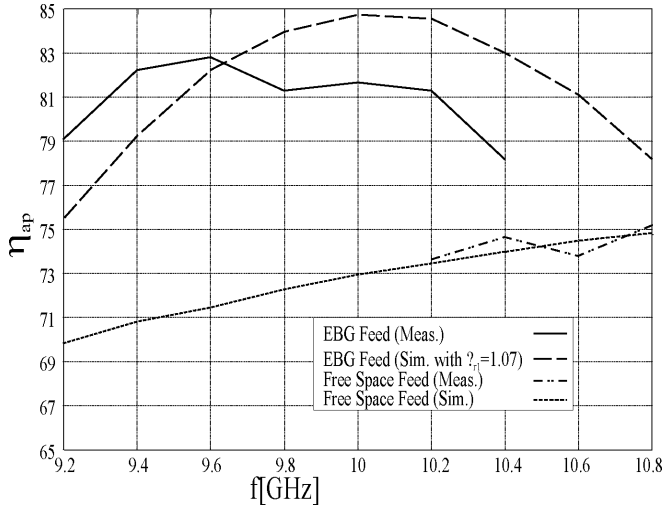

Fig. 15. Measured aperture efficiency as a function of the frequency.

on the applicability of the concept presented are in order. An apparent problem of the proposed solution is that the large dimension of the dielectric slabs that will induce blockage. This blockage has been considered in the final efficiency figures. Since a competing horn feed could imply a smaller blockage, the EBG feed would be attractive for applications that require large reflectors ($G > 45$ dBi) in which the aperture efficiency is a critical design parameter.

In other realistic scenarios there is a clear tendency to select off set configurations rather than central fed ones. To tackle these configurations the same procedure used in this article could be applied starting from non symmetric feed patterns.

The major advantage of this design procedure is that the waveguide aperture is very small. The extension to an array configuration is then simple, which opens up the possibility of multi beam system. Such systems have been recently developed in the frame of the extension of the present work to a specific satellite based, multibeam telecommunication application. The preliminary results are anticipated in [15].

APPENDIX

The spectral dyadic Green's function associated to the electric $\mathbf{E}$ fields in (x, y, z) radiated in the region of space above the EBG dielectric stratifications by a magnetic current $\mathbf{m}(x', y')$ can be expressed as follows:

$$\underline{\underline{\mathbf{G}}}^{\mathrm{em}}(k_x, k_y, z) = \begin{bmatrix} \frac{k_x k_y (V_{\mathrm{TM}}(k_\rho) - V_{\mathrm{TE}}(k_\rho))}{k_\rho^2} & \frac{-(k_x^2 V_{\mathrm{TM}}(k_\rho) + k_y^2 V_{\mathrm{TE}}(k_\rho))}{k_\rho^2} \\ \frac{(k_y^2 V_{\mathrm{TM}}(k_\rho) + k_x^2 V_{\mathrm{TE}}(k_\rho))}{k_\rho^2} & \frac{k_x k_y (V_{\mathrm{TE}}(k_\rho) - V_{\mathrm{TM}}(k_\rho))}{k_\rho^2} \\ -\frac{k_y V_{\mathrm{TM}}(k_\rho)}{k_{z0}} & \frac{k_x V_{\mathrm{TM}}(k_\rho)}{k_{z0}} \end{bmatrix} \quad (6)$$

where V_{TM} and V_{TE} are the voltage solutions of TM and TE transmission line representing the stratification in the z direction with a unitary series voltage generators. $k_\rho = \sqrt{k_x^2 + k_y^2}$ is the radial spectral variable that is introduced by the double change of variable $k_x = k_\rho \cos\alpha$ and $k_y = k_\rho \sin\alpha$ leading to $\alpha = \arctan(k_y/k_x)$.

The spectral dyadic Green's function associated to the magnetic $\mathbf{H}$ field in $(x, y, z = 0)$ radiated by a magnetic current $\mathbf{m}(x', y')$ can be expressed as follows:

$$\underline{\underline{\mathbf{G}}}^{hm}(k_x, k_y, z) = \begin{bmatrix} \frac{-(k_x^2 I_{\mathrm{TE}}(k_\rho) + k_y^2 I_{\mathrm{TM}}(k_\rho))}{k_\rho^2} & \frac{k_x k_y (I_{\mathrm{TM}}(k_\rho) - I_{\mathrm{TE}}(k_\rho))}{k_\rho^2} \\ \frac{k_x k_y (I_{\mathrm{TM}}(k_\rho) - I_{\mathrm{TE}}(k_\rho, z, z'))}{k_\rho^2} & \frac{-(k_y^2 I_{\mathrm{TE}}(k_\rho) + k_x^2 I_{\mathrm{TM}}^m(k_\rho))}{k_\rho^2} \end{bmatrix} \quad (7)$$

where I_{TM} and I_{TE} are the current solutions of TM and TE transmission line representing the stratification in the z direction with a unitary series voltage generators.

ACKNOWLEDGMENT

Thanks are expressed to F. Nennie for performing the measurements.

REFERENCES

[1] Y. Rahmat-Samii, "Reflector antennas," in *Antenna Handbook*, Y. T. Lo and S. W. Lee, Eds. New York: Van Nostrand Reinhold, 1988, ch. 15.

[2] A. Cha and D. Bathker, "Preliminary announcement of an 85 percent efficient reflector antenna," *IEEE Trans. Antennas Propag.*, vol. 31, pp. 341–342, Mar. 1983.
[3] C. Cheype, C. Serier, M. Thevenot, T. Monediere, A. Reineix, and B. Jecko, "An electromagnetic bandgap resonator antenna," *IEEE Trans. Antennas Propag.*, vol. 50, pp. 1285–1290, Sep. 2002.
[4] Y. J. Lee, J. Yeo, R. Mittra, and W. S. Park, "Application of electromagnetic bandgap auperstrates with controllable defects for a class of patch antennas as spatial angular filters," *IEEE Trans. Antennas Propag.*, vol. 53, pp. 224–235, Jan. 2005.
[5] N. Guerin, S. Enoch, G. Tayeb, P. Sabouroux, P. Vincent, and H. Legay, "A metallic Fabry–Perot directive antenna," *IEEE Trans. Antennas Propag.*, vol. 54, pp. 220–224, Jan. 2006.
[6] R. Gardelli, M. Albani, and F. Capolino, "Array thinning by using antennas in a Fabry–Perot cavity for gain enhancement," *IEEE Trans. Antennas Propag.*, vol. 54, pp. 1979–1990, Jul. 2006.
[7] Balanis Antenna Theory: Analysis and Design. New York, Wiley Interscience, 2005.
[8] N. L. Juan, "Development of integrated printed array antennas using EBG substrates," Ph.D. dissertation, Technical University of Valencia, Spain.
[9] T. Zhao, D. R. Jackson, J. T. Williams, and A. A. Oliner, "General formulas for 2-D leaky-wave antennas," *IEEE Trans. Antennas Propag.*, vol. 53, pp. 3525–3533, Nov. 2005.
[10] D. R. Jackson, A. A. Oliner, and A. Ip, "Leaky wave propagation and radiation for a narrow-beam multiple layer dielectric structure," *IEEE Trans. Antennas Propag.*, vol. 41, pp. 344–348, Mar. 1993.
[11] G. Lovat, P. Burghignoli, and D. R. Jackson, "Fundamental properties and optimization of broadside radiation from uniform leaky-wave antennas," *IEEE Trans. Antennas Propag.*, vol. 54, pp. 1442–1452, May 2006.
[12] D. R. Jackson and A. A. Oliner, "A leaky-wave analysis of the high-gain printed antenna configuration," *IEEE Trans. Antennas Propag.*, vol. 36, pp. 905–909, Jul. 1988.
[13] A. Neto, R. Bolt, G. Gerini, and D. Schmidt, "Multimode equivalent network for the analysis of a radome covered finite array of open ended waveguides," presented at the IEEE/AP-S URSI Meeting, Columbus, OH, Jun. 22-27, 2003.
[14] CST Microwave Studio, User Manual Version 5.0. Darmstadt, Germany, CST GmbH.
[15] M. Bonnedal, N. Llombart, A. Neto, G. Gerini, and P. de Maagt, "Leaky wave enhanced feeds in multibeam reflector antennas: The radiometric and telecom scenarios," in *Proc. 29th ESA Antenna Workshop on Multiple Beams and Reconfigurable Antennas*, Noordwijk, The Netherlands, Apr. 18-20, 2007.

Andrea Neto (M'00) received the Laurea degree (*summa cum laude*) in electronic engineering from the University of Florence, Florence, Italy, in 1994 and the Ph.D. degree in electromagnetics from the University of Siena, Siena, Italy, in 2000.

Part of his Ph.D. was developed at the European Space Agency Research and Technology Center, Noordwijk, The Netherlands, where he worked for over two years in the Antenna Section. From 2000 to 2001, he was a Postdoctoral Researcher at the California Institute of Technology, Pasadena, working for the Sub-millimeter Wave Advanced Technology Group (S.W.A.T.) Group of the Jet Propulsion Laboratory. Since 2002, has been a Senior Antenna Scientist at the Defence, Security and Safety Institute of The Netherlands Organization for Applied Scientific Research (TNO), The Hague, The Netherlands. His research interests are in the analysis and design of antennas, with emphasis on arrays, dielectric lens antennas, wideband antennas and EBG structures.

Nuria Llombart (S'06–M'07) received the Ingeniero de Telecomunicación degree and the Ph.D. degree from the Universidad Politécnica de Valencia, Spain, in 2002 and 2006, respectively.

During her Master's degree studies she spent one year at the Friedrich-Alexander University of Erlangen-Nuremberg, Germany, and worked at Fraunhofer Institute for Integrated Circuits in Erlangen, Germany. From 2002 until 2007, she was with the Antenna Unit at the Defence, Security and Safety Institute of the Netherlands Organization for Applied Scientific Research (TNO) in The Hague, The Netherlands, working as a Ph.D. student and afterwards as a Researcher. Currently, she is a Postdoctoral Fellow at the California Institute of Technology, Pasadena, working for the Sub-millimeter Wave Advanced Technology Group (S.W.A.T.) Group of the Jet Propulsion Laboratory. Her research interests include the analysis and design of printed array antennas, EBG structures, and reflector antennas.

Dr. Llombart's Ph.D. was financed and hosted by the Defence, Security and Safety Institute of the Netherlands Organization for Applied Scientific Research (TNO) in The Hague, The Netherlands

Giampiero Gerini (M'92) received the M.S. degree (*summa cum laude*) and the Ph.D. degree in electronic engineering from the University of Ancona, Ancona, Italy, in 1988 and 1992, respectively.

From 1994 to 1997, he was a Research Fellow at the European Space Research and Technology Centre (ESA-ESTEC), Nooordwijk, The Netherlands, where he joined the Radio Frequency System Division. Since 1997, he has been with the Netherlands Organization for Applied Scientific Research (TNO), The Hague, The Netherlands. At TNO Defence, Security and Safety, he is currently Chief Senior Scientist of the Antenna Unit in the Transceivers and Real-time Signal Processing Department. His main research interests are phased array antennas, frequency selective surfaces and integrated front-ends.

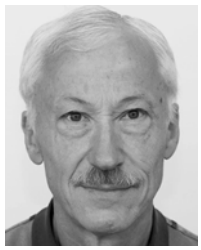

Magnus D. Bonnedal (M'74) received the M.Sc. degree in electrical engineering and the Ph.D. degree in plasma physics from Chalmers University of Technology, Gothenburg, Sweden, in 1972 and 1979, respectively.

He has since been working at Ericsson and Saab Space, Goteborg, Sweden, with the development of arrays, reflector antennas and feed systems in communication and earth observation applications. He is presently engaged in the development of navigation receivers for satellite precise orbit determination and earth observation.

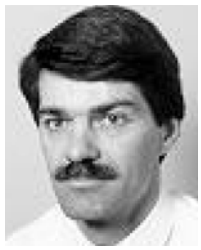

Peter de Maagt (S'88–M'88–SM'02) was born in Pauluspolder, The Netherlands, in 1964. He received the M.Sc. and Ph.D. degrees from Eindhoven University of Technology, Eindhoven, The Netherlands, in 1988 and 1992, respectively, both in electrical engineering.

He is currently with the European Space Research and Technology Centre (ESTEC), European Space Agency, Noordwijk, The Netherlands. His research interests are in the area of millimeter and submillimeter-wave reflector and planar integrated antennas, quasi-optics, photonic bandgap antennas, and millimeter- and sub-millimeter-wave components.

Dr. de Maagt was a co-recipient of the H. A. Wheeler award of the IEEE Antennas and Propagation Society for the Best Applications Paper in 2001. He was granted a European Space Agency award for innovation in 2002.